How to cite: *Angew. Chem. Int. Ed.* **2025**, *64*, e202505897
doi.org/10.1002/anie.202505897

Polycyclic Hydrocarbons

Azuperylene: The Nonalternant Isomer of Perylene

Shengpei Liu, Marcos Díaz-Fernández, Menglin Zhang, Fei Huang, Yong Chen, Yudong Yang, José Manuel Marín-Beloqui, Jingbo Lan, Jingsong You, Juan Casado,* and Cheng Zhang**

Abstract: The isoelectronic isomer of perylene, hereafter called as azuperylene, has been prepared. Electronic structure analysis reveals that the new isomer can be described as a union of two antiparallel azulenes in which the azulene-type aromatic character of the starting azulene is partially retained. Four 2,8-dialkoxy (i.e., ethoxy, *n*-butoxy, *n*-hexyloxy, and *n*-octyloxy) functionalized derivatives of the new isomer core have been prepared. The solid-state structures of the new compounds have been resolved showing exceptional herringbone π–π stacking ideal for charge transport. Organic field-effect transistors on sublimated substrates display an excellent hole transport mobility up to 1.03 $cm^2 V^{-1} s^{-1}$ that largely surpasses that of perylene and reveals the great potential for charge transport of this new class of nonbenzenoid compounds.

Introduction

Organic semiconductors[1–3] have garnered considerable attention due to their potential applications in organic field-effect transistors (OFETs),[4–6] organic light-emitting diodes (OLEDs),[7,8] and organic photovoltaics (OPVs).[9] Some examples are diketopyrrolopyrrole (DPP),[10,11] benzothieno[3,2-*b*] benzothiophene (BTBT),[12–14] and perylene diimide (PDI).[15–17] Given the advantages of structural diversity of organic molecules and their relative ease of modification, rational development of novel organic π-conjugated building blocks to expand and improve the library of organic semiconducting materials is mandatory. π-Conjugated polycyclic fused aromatic hydrocarbons (PAHs) are the prototypical molecules for organic optoelectronics.[18–20] In this regard, π-conjugated systems can be classified into alternant and nonalternant molecules; whereas alternant molecules have been extensively used in the field, nowadays, nonalternant molecules are receiving increasing attention.[21–24] The textbook examples of parent alternant and nonalternant molecular isomers are naphthalene (benzenoid) and azulene (nonbenzenoid). As an isomer of naphthalene, azulene is formed by fusing an electron-deficient seven-membered ring and an electron-rich five-membered ring, exhibiting nonmirror-symmetric frontier molecular orbitals, which endows azulene with a smaller bandgap and a large dipole moment (i.e., 1.08 D).[25–27]

Compared to the highly reactive five-membered ring of azulene, its seven-membered ring is chemically inert in most of its positions, resulting in a limitation in the way to design azulene derivatives. Hence, azulene functionalization is carried out at the 1,2,3-positions of the five-membered ring and at the sole 6-position on the seven-membered ring (Scheme 1a). The current interest in the development of new azulene derivatives runs in parallel with the growing interest in nonbenzenoid ring-containing PAHs.

For instance, 1,8-azulene-containing derivatives in Scheme 1b have been reported as embedded moieties in higher order planar PAHs through peripheral expansion of a five-membered ring or seven-membered ring via alkyne cyclization or Scholl reactions, respectively.[28–31] However, rather than beginning from one already functionalized azulene precursor, it is challenging to directly functionalize azulene for the preparation of new azulene-based PAHs. In this regard, following the argument of azulene as an electronic isomer of naphthalene, we now present the unprecedented formation of the azulene-based isomer of perylene, dicyclohepta[*cd,ij*]-*s*-indacene (that we will refer to as azuperylene by its relationship to perylene and will denote as **AP**, i.e., **azup**erylene). **AP** results from the antiparallel union of two azulenes with a centrosymmetric symmetry. Along these lines, the parallel azulene-dimer parent (i.e., non-centrosymmetric isomer of **AP**) has been recently prepared, though its properties are completely different compared to those of **AP**.[32,33] Other azulene dimers have been reported in the form of PAHs containing **AP** where the role of the **AP** moiety is minorized by the massive fusion with other rings in these larger PAHs.

Perylene is the centrosymmetric nonfused dimer of naphthalene and its derivatives have been largely studied and

[*] S. Liu, M. Zhang, F. Huang, Y. Chen, Prof. Y. Yang, Prof. J. Lan, Prof. J. You, Prof. C. Zhang
Key Laboratory of Green Chemistry and Technology of Ministry of Education, College of Chemistry, Sichuan University, 29 Wangjiang Road, Chengdu 610064, P.R. China
E-mail: jsyou@scu.edu.cn
cheng.zhang@scu.edu.cn

M. Díaz-Fernández, J. M. Marín-Beloqui, Prof. J. Casado
Department of Physical Chemistry, University of Malaga, Campus de Teatinos s/n, Málaga 29071, Spain
E-mail: casado@uma.es

Additional supporting information can be found online in the Supporting Information section

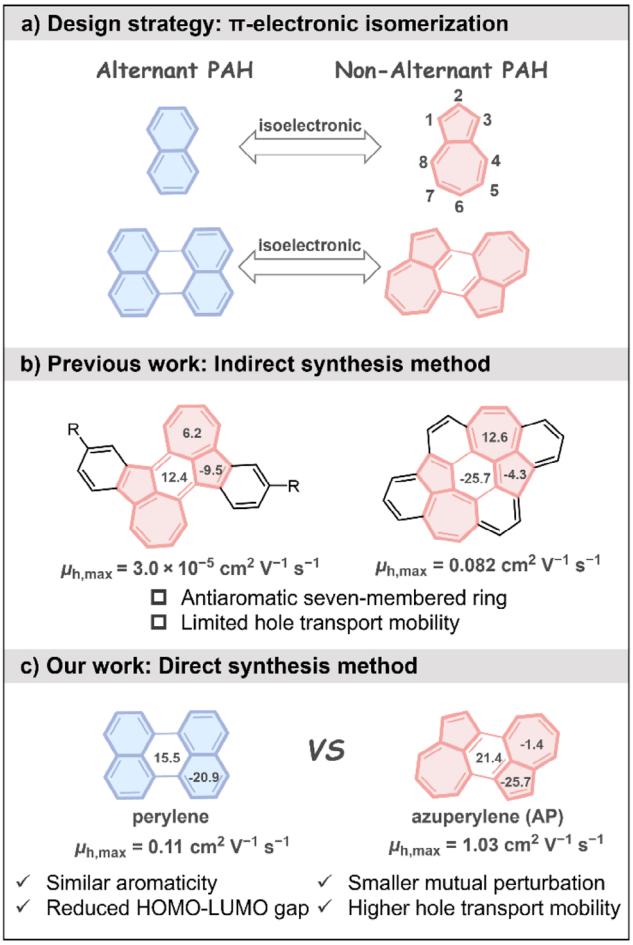

Scheme 1. Centrosymmetric reported molecules containing nonbenzenoid rings and our molecular design strategy based on azulene. The numbers within the rings are NICS values (see below). $\mu_{h,max}$, maximum hole mobility; HOMO, highest occupied molecular orbital; LUMO, lowest unoccupied molecular orbital.

implemented in organic optoelectronic applications.[8,19,34] As a further attempt to find new π-conjugated systems, to the best of our knowledge, the centrosymmetric π-electronic isomer of perylene, **AP** in Scheme 1c, has not been prepared. **AP** might have a threefold interest: i) from a conceptual perspective, it is highly valuable to gain further insights into the understanding of the evolution of the electronic structure upon isomerization from alternant/benzenoid to nonalternant/nonbenzenoid structures; ii) it poses a synthetic challenge; and iii) its potential incorporation as a new organic semiconductor in organic devices.

In particular, herein, we developed a palladium-catalyzed annulative C−H/C−I coupling reaction at the 1- and 8-positions of azulene to form **AP**s. Furthermore, we inspect the electronic structure of **AP** in comparison with azulene and perylene and will discuss the modulation of its electronic structure with substitution. The solid-state crystal packings of **AP** and its derivatives together with the charge transport behavior are also addressed. Indeed, the new compounds were incorporated as semiconducting substrates in OFET devices and a maximum hole mobility of 1.03 $cm^2 V^{-1} s^{-1}$ was

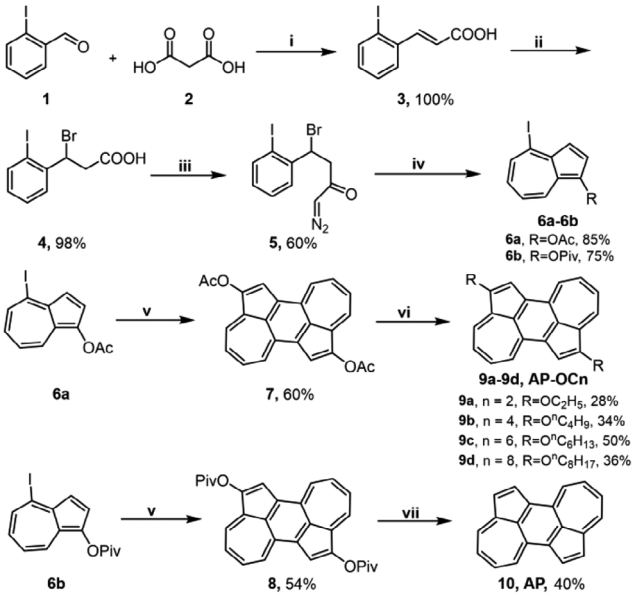

Figure 1. Synthesis routes of **AP** and its derivatives. i) Piperidine, pyridine, 120 °C. ii) HBr, AcOH, 96 h. iii) (1) Oxalyl chloride, benzene, 65 °C, 18 h; (2) $TMSCHN_2$, MeCN, 0–4 °C, 24 h. iv) (1) $Rh_2(OCOt\text{-}Bu)_4$, r.t.; (2) AcO_2/pivaloyl chloride, 4-dimethylaminopyridine, r.t. v) $PdCl_2$, PPh_3, CsOAc, CPME, 120 °C, 16 h. vi) Alkyl bromide, Cs_2CO_3, MeOH, DMF. vii) $Ni(cod)_2$, dcype, HCOONa, toluene.

achieved, which is 10 times higher than that of its isoelectronic perylene isomer (Scheme 1c).

Results and Discussion

Synthesis of APs

In the past two decades, transition metal catalyzed direct C−H arylation has emerged as a powerful tool to rapidly assemble diverse PAHs from simple synthetic blocks. This revolutionary synthetic strategy may provide a completely different retrosynthetic opportunity for the construction of complex structures.[35–37] Indeed, the retrosynthetic analysis of the targeted **AP** suggested that the central benzene ring could be produced by an annulative C−H/C−X coupling between two halo azulene units.

As shown in Figure 1, starting from the simple substituted benzaldehyde, the Knoevenagel condensation reaction with malonic acid was performed to quantitatively generate (*E*)-3-(2-iodophenyl) propenoic acid **3**, which was then added to the HBr/AcOH solution to obtain 3-(2-iodophenyl)propanoic acid **4** with a yield of 98%. Subsequently, consecutive reactions with oxaloyl chloride and trimethylsilyldiazomethane provided 4-bromo-4-(2-iodophenyl)-1-diazo-2-butanone **5** in a 60% yield. Next, ring expansion-annulation[38] in the presence of rhodium delivered iodoazulene **6a** and **6b** in 85% and 75% yields, respectively. However, the following annulative C−H/C−X coupling between iodoazulenes proved to be challenging. No desired product was detected in the catalysis of $Pd(OAc)_2$ and quaternary ammonium salts in *N*,*N*-dimethylformamide (DMF), which were common

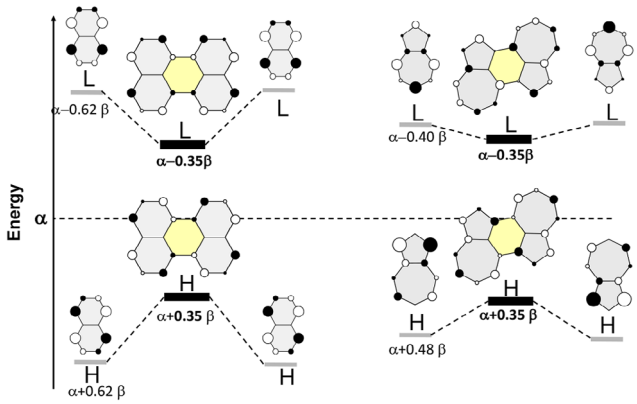

Figure 2. Hückel frontier molecular orbital energies and atomic compositions of perylene and **AP** as generated by a combination of naphthalene and azulene, respectively. H, HOMO; L, LUMO.

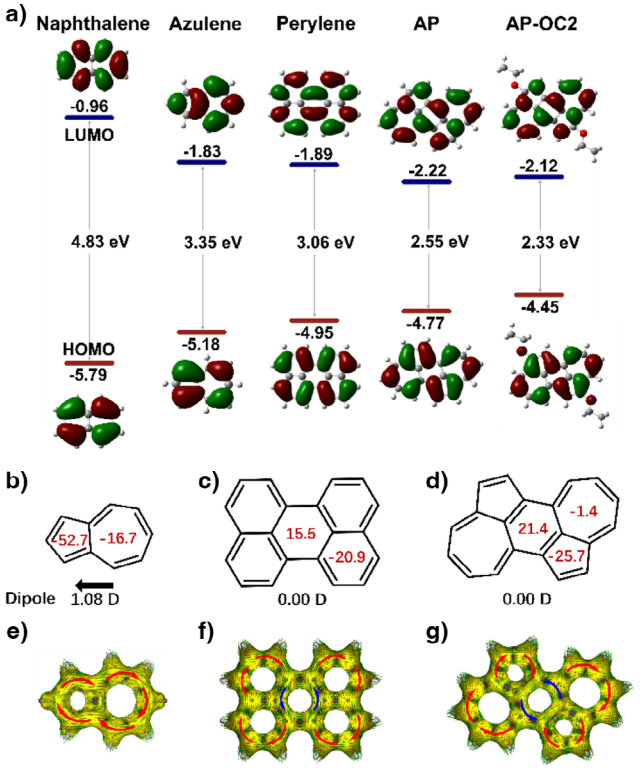

Figure 3. a) Calculated molecular orbital distributions and orbital energy levels of naphthalene, azulene, perylene, **AP**, and **AP-OC2**. b) and d) NICS(1)$_{zz}$ values and e)–g) ACID-derived induced ring current maps of (b and e) azulene, (c and f) perylene, and (d and g) **AP**.

catalytic systems in the C–H/C–I coupling between arenes.[39] This result indicated the different reactivity of azulenes from that of benzenoid analogues in direct C–H arylation. Thus, the reaction conditions for the direct annulative coupling were explored (Table S1). Solvent was demonstrated to have a pivotal effect on the yields. Toluene and cyclopentyl methyl ether (CPME) proved to be the most suitable solvents in our tests (Table S1, Entries 13 and 34). After further screening of various reaction parameters, such as palladium sources, bases, ligands and solvents, the reaction conducted with $PdCl_2$ as the catalyst, PPh_3 as the ligand, CsOAc as the base, and CPME as the solvent at 120 °C could afford the **AP** derivatives **7** and **8** in 60% and 54% yields, respectively (Figure 1 and Table S1, Entry 14). Notably, the reaction of **6b** on a gram-scale delivered **8** in a 42% yield, suggesting the synthetic scalability of this reaction (see Supporting Information). More importantly, the acetoxy (OAc-) and pivalate (OPiv-) substituents on **9** and **10** could be substituted by alkoxy-chain and hydrogen to afford **AP-OCn** (**9a-d**) and **AP** (**10**). The decomposition temperature of **9a** and **10** were determined to be 210 and 189 °C, respectively (Figure S5). The facile transformation of these functionalities facilitates the arbitrary modification of the stacking modes of azuperylenes, which is highly crucial in the development of high performance OFET materials.

Electronic Structure: Energy Level and Aromaticity of APs

Figure 2 displays the evolution of the π-electronic structure from the perturbative Hückel molecular orbital method considering of **AP** as the union of two azulenes. Overall, the highest occupied molecular orbital (HOMO) and lowest unoccupied molecular orbital (LUMO) of **AP** are formed from the combinations of the HOMOs and LUMOs of two azulenes, respectively. Given that the formation of the two new bonds in **AP** connecting the azulenes involves carbon atoms with small atomic π-coefficients, the interazulene coupling produces a limited alteration of the energies of the frontier molecular orbitals of **AP** compared to azulene. This is relevant as **AP** can be considered as the sum of two azulenes. The same Hückel type calculations have been carried out for perylene in Figure 2 where it is observed that the formation of the two CC bonds from naphthalene occurs between atoms with larger π-coefficients. This discussion reveals that the mutual perturbation of two naphthalenes (i.e., to form perylene) is larger than that of two azulenes (i.e., to form **AP**), in such a way that although the HOMO–LUMO gap in azulene is smaller than that of naphthalene, in perylene and in **AP** this becomes equal (at the Hückel level). Upon inclusion of electron correlation at the density functional theory (DFT) level, the situation changes (Figure 3a) and the HOMO–LUMO energy gap in **AP** is 0.51 eV smaller than in perylene.

Either for the Hückel and DFT models, medium-size atomic coefficients are predicted for the carbon atoms of the five-membered rings (i.e., where functionalization takes place from **AP** to **AP-OCn**) in the HOMO, whereas these coefficients are vanishing in the LUMO of **AP**. This indicates that functionalization with donor groups in these positions would destabilize the HOMO orbitals owing to the conjugative effect of the lone electron pair of the oxygen toward the π-core, as can be seen in Figure 3a with HOMO energy values of −4.77 eV in **AP** and −4.45 eV in **AP-OC2**; whereas the effect on the energies of the LUMO is much smaller: −2.22 eV in **AP** and −2.12 eV in **AP-OC2**. This conjugative effect on **AP** → **AP-OC2** narrows the HOMO–LUMO gap that will affect the optical properties.

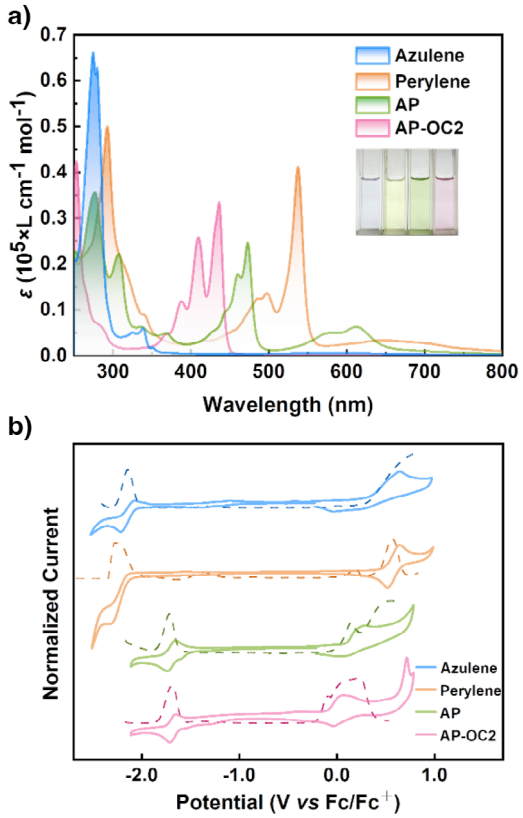

Figure 4. a) Absorption spectra of azulene, perylene, **AP**, and **AP-OC2** in CH_2Cl_2 (1.0×10^{-5} M). b) Cyclic voltammetry (solid lines) and differential pulse voltammetry (dashed lines) of azulene, perylene, **AP**, and **AP-OC2** in dry CH_2Cl_2 (1.0×10^{-3} M) containing 0.1 M Bu_4NPF_6.

Considering **AP** and perylene as a pair of centrosymmetric isoelectronic species, the nucleus-independent chemical shift (NICS) by DFT calculations and anisotropy of the current-induced density (ACID) analysis were conducted. As shown in Figure 3b–g, the negative NICS(1)$_{zz}$ value and the clockwise ring currents (red circle) on the five- and seven-membered rings in **AP** indicate aromatic characters, consistent with the molecular orbital interpretation of **AP** as two joint azulenes. Besides, due to the antiparallel or centrosymmetric connection of the two azulenes, the dipole moment of **AP** is nullified (0.004 D).

Absorption Spectra and Electrochemical Properties

Figure 4a illustrates the comparison of the absorption spectra of azulene, perylene**,** **AP**, and **AP-OC2** in diluted dichloromethane solutions. Upon expansion of π-conjugated core on azulene→**AP** / **AP-OC2**, the absorption bands of the latter exhibit the typical redshift compared with azulene. The strongest absorption bands of the compounds appear at 437 nm in perylene (assigned by TD-DFT to the $S_0 \rightarrow S_1$ excitation and predicted at 428 nm with oscillator strength of 0.36, Figure S9), at 474 nm in **AP**, and at 538 nm in **AP-OC2** (in both cases assigned to the $S_0 \rightarrow S_4$ excitations and predicted at 443 and 479 nm with oscillator strengths of 0.24 and 0.33 in **AP** and **AP-OC2**, respectively, Figure S9).

For **AP**, there are three medium–weak bands at 570, 610, and 680 nm (assigned to the $S_0 \rightarrow S_3$, $S_0 \rightarrow S_2$ and $S_0 \rightarrow S_1$ excitations, respectively, and calculated by TD-DFT at 547, 569, and 639 nm all with small oscillator strengths, Figure S9). In **AP-OC2**, these three low energy bands have the same assignment as in **AP** and appear at 610, 640, and 700 nm. These three weak bands of **AP** and **AP-OC2** can be correlated with that of azulene at 580 nm corresponding to a very broad and weak band due to the $S_0 \rightarrow S_1$ excitation. The overall redshift from **AP** to **AP-OC2** can be related with the destabilization of the HOMO by including donor groups due to conjugation of the lone electron pair of the oxygens and the subsequent narrowing of the HOMO–LUMO gap such as explained above. As a result, the resulting colors of the solutions of azulene, perylene**,** **AP**, and **AP-OCn** vary from blue, yellow, green, and pink, respectively.

Electrochemical properties were investigated by cyclic voltammetry and the redox potentials were calibrated against a ferrocene/ferrocenium (Fc/Fc^+) couple as the internal standard (Figure 4b). The HOMO energy levels of azulene, perylene,[40] **AP,** and **AP-OC2** are determined to be −5.43, −5.60, −5.20, and −5.00 eV, whereas the LUMO energy levels are −3.03, −3.36, −3.59 and −3.51 eV, respectively. The variation of the values of the LUMO from calculations in the four compounds follows well the tendency found experimentally for the LUMO values from cyclic voltammetry.

Single-Crystals Structures

We have obtained the single-crystals of **AP** and of **AP-OC2** and other derivatives[41] for X-ray single-crystal analysis (Figures 5 and S1), which were prepared through the volatilization method in chloroform solution and by the diffusion method in which with methanol diffuses into chloroform or toluene (detailed crystallographic data are summarized in Tables S2–S5).

These crystal structures all demonstrate a planar geometry of the **AP** core. As shown in Figure S3, the bond lengths of azulene unit of **AP** are almost identical to that of azulene. Accordingly, the harmonic oscillator measure of aromaticity (HOMA) values for the azulene moiety of **AP** are similar to those of pristine azulene. It is observed herringbone packings in **AP** and **AP-OC2** with typical π–π stacking distances (i.e., other **AP** derivatives such as **AP-OC6** and **AP-OC8** present layered structures without ***π–π*** stacking and hence potentially inferior for charge transport). By comparing the herringbone packing modes of **AP** and **AP-OC2**, it can be observed that **AP** stacks in a dimer fashion, similar to the α-phase of perylene,[42–44] with a π–π distance of 3.47 Å and a titled angle to the adjacent dimer of 87°. Furthermore, **AP** shows a face-to-face disposition of the seven- and five-membered rings in the intermolecular dimer. Meanwhile, **AP-OC2** presents a monomer-type herringbone arrangement with a shorter ***π–π*** distance of 3.36 Å. The closer π–π distance of **AP-OC2** can be ascribed to the reinforced electrostatic interactions between the

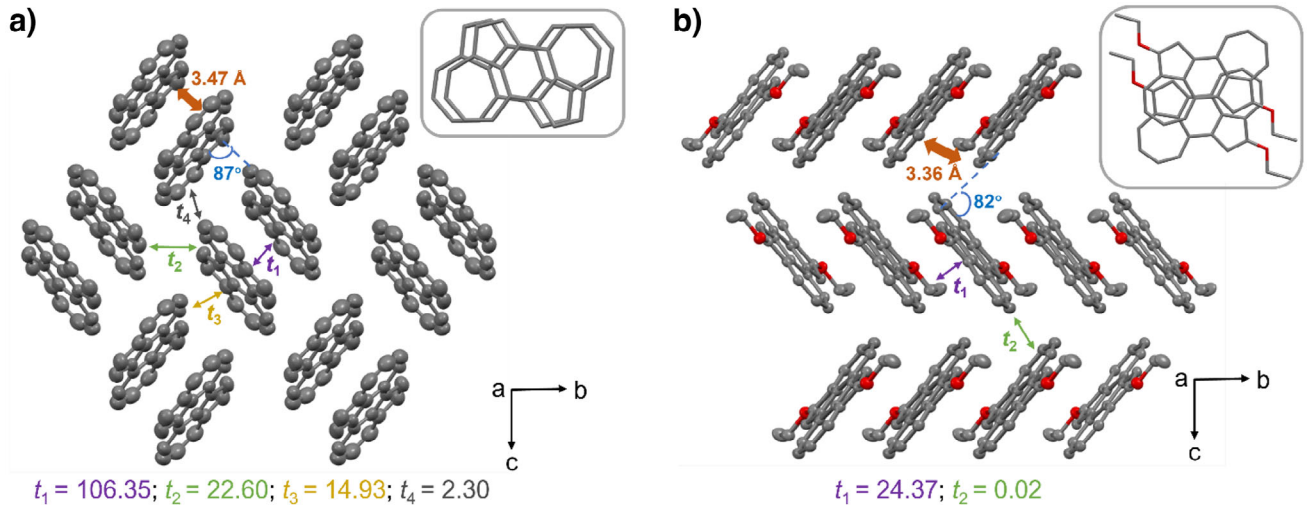

Figure 5. X-ray single-crystal packings of a) **AP** and b) **AP-OC2**. The inserted figures and t_n values (meV) in (a) and (b) represent the packing modes of dimers and the calculated transfer integrals for holes, respectively.

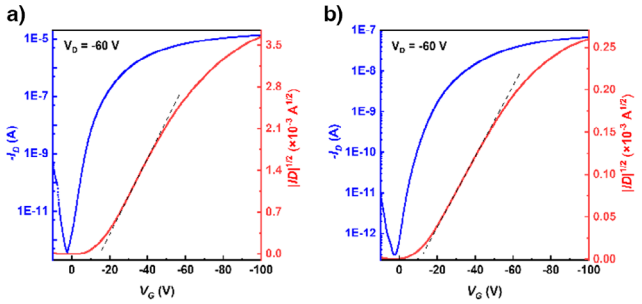

Figure 6. Transport curves based on a) **AP** and b) **AP-OC2** single-crystal FET devices.

electron-deficient seven-membered rings facing the electron-rich five-membered rings upon inclusion of alkoxy donor. In contrast, this antiparallel intermolecular arrangement in **AP-OC2** leads to an apparent less effective π–π overlap due to the asymmetrical intermolecular orbital couplings (see Figure S8 for a detailed analysis of the intermolecular interactions by means of a Hirshfeld surface analysis).

Organic Field-Effect Transistors

Bottom-gate top-contact (BGTC) single-crystal OFET devices were fabricated to assess the semiconducting properties of **AP** and **AP-OC2**. The single-crystals were sublimated onto octadecyltrichlorosilane (OTS)-modified SiO_2 (300 nm)/Si substrates through physical vapor transfer (PVT) methods, followed by the vacuum deposition of gold to serve as source and drain electrodes. The mobility is calculated in the saturation current regimes, such as shown in Figures 6 and S11 and summarized in Table S10. Both **AP** and **AP-OC2** exhibit typical p-type charge transport characteristics. Compared with **AP-OC2** showing the hole mobility up to 0.078 cm^2 V^{-1} s^{-1}, the devices based on **AP** exhibit the highest hole mobility reaching 1.03 cm^2 V^{-1} s^{-1}, with an I_{on}/I_{off} of 10^9 and a threshold voltage (V_T) of −9.4 V. Compared to other azuperylene-embedded molecules reported previously, **AP** with a smaller molecular weight performs much better in hole transport regime than all its parents. On the other hand, it displays a notable improvement in hole transport compared to perylene (0.11 cm^2 V^{-1} s^{-1}). Transfer integrals and reorganization energies (Table S9) of **AP** and **AP-OC2** were theoretically calculated based on their crystal data. The largest transfer integrals (t_1, Figure 5) for holes of **AP** and **AP-OC2** are all from the dimers with π–π stacking with values of 106.4 and 24.4 meV, respectively. Compared to t_1, t_2 in **AP** is smaller (22.6 meV), but is vanishing and residual in **AP-OC2** (0.02 meV), revealing that **AP-OC2** only possesses a 1D channel for charge transport. Conversely, **AP** shows an additional third channel, t_3 = 14.9 meV, highlighting a situation of 3D channel transport in **AP** crystals. Besides, β-phase perylene with only C–H···π interactions results in limited transfer integrals (Figure S2) and hole mobilities. Combined with the lower hole reorganization energy of 121.22 meV in **AP**, which is in the energy order of the best hole organic semiconductors (i.e., pentacene), this study presents **AP** as a promising nonbenzenoid class building block for achieving high-performance semiconductors.

Conclusion

Here, we have prepared the odd-member ring based centrosymmetric isomer of perylene (i.e., azuperylene). As a novelty, we developed C–H/C–I coupling reactions based on 1,8-azulene that ultimately result in the formation of azuperylene with the versatility to produce some functionalized azuperylenes in the same reaction code. The electronic structure of azuperylene can be described as two joint azulenes with weak perturbation in between and therefore retaining the segmented azulene-like aromatic character in their five- and seven-membered rings. The absorption properties of

azuperylene remind those of azulene with a set of weak low-energy absorption bands in the visible region close to the NIR. The solid-state structure of the new derivatives reveals a main herringbone π–π crystal packing that is the optimal situation for transport behavior. Indeed, OFET devices, using the unfunctionalized azuperylene (i.e., that with maximal π-π overlap) as semiconducting substrate, display exceptional semiconducting properties with a maximum hole mobility of 1.03 $cm^2\ V^{-1}\ s^{-1}$. Azuperylene represents one of the first nonbenzenoid nonalternant PAH compounds with notable semiconducting performance, even superior to the well-established perylene isomer. This evolution of the semiconducting performance on passing from benzenoid to nonbenzenoid compounds is of great significance in the field toward diversified molecules in organic electronics.

Supporting Information

Supporting Information is available from the Wiley Online Library, including synthesis details; analytical data obtained by mass spectrometry and NMR; results of single-crystal X-ray analysis, spectroscopic characterization, theoretical calculations, and OFET device fabrication.

Acknowledgements

C.Z., Y.Y. J.L., and J.Y. acknowledge the financial support from the National Natural Science Foundation of China with Grant No. 22205150 (C.Z.), 2025ZNSFSC0117 (Y.Y.), 22071162 (J.L.), 22031007 (J.Y.), the Sichuan Science and Technology Program with Grant No. 2024JDRC0009 (C.Z.), and the Fundamental Research Funds for the Central Universities (C.Z.). The authors also thank Jing Li and Meng Yang from the Comprehensive Training Platform Specialized Laboratory, College of Chemistry, Sichuan University, for compound characterizations. M.D.-F. acknowledges the Spanish Science and Innovation Ministry for his FPI fellowship. J.C. thanks the Junta de Andalucía (Project Reference PROYEXC-0328, P21-0328) and Ministerio de Ciencia, Innovación y Universidades of Spain (Project Reference PID2024-157601NB-I00) for financial support.

Conflict of Interests

The authors declare no conflict of interest.

Data Availability Statement

The data that support the findings of this study are available from the corresponding author upon reasonable request.

Keywords: Azulene · Electronic isomers · organic semiconductors · polycyclic aromatic hydrocarbons · Perylene

[1] J. Cheng, W. Zhang, L. Wang, G. Yu, *Adv. Mater.* **2023**, *35*, 2210772.
[2] C. Wang, H. Dong, L. Jiang, W. Hu, *Chem. Soc. Rev.* **2018**, *47*, 422–500.
[3] Z. Xie, D. Liu, C. Gao, H. Dong, W. Hu, *Nat. Rev. Mater.* **2024**, *9*, 837–839.
[4] H. Jiang, S. Zhu, Z. Cui, Z. Li, Y. Liang, J. Zhu, P. Hu, H.-L. Zhang, W. Hu, *Chem. Soc. Rev.* **2022**, *51*, 3071–3122.
[5] J. Li; Z. Chen, J. Wang, S. Young Jeong, K. Yang, K. Feng, J. Yang, B. Liu, H. Y. Woo, X. Guo, *Angew. Chem. Int. Ed.* **2023**, *62*, e202307647.
[6] Z. Liu, W. Han, J. Lan, L. Sun, J. Tang, C. Zhang, J. You, *Angew. Chem. Int. Ed.* **2022**, *62*, e202211412.
[7] G. Hong, X. Gan, C. Leonhardt, Z. Zhang, J. Seibert, J. M. Busch, S. Bräse, *Adv. Mater.* **2021**, *33*, 2005630.
[8] Y. Wu, X. Liu, J. Liu, G. Yang, Y. Deng, Z. Bin, J. You, *J. Am. Chem. Soc.* **2024**, *146*, 15977–15985.
[9] C. Yan, S. Barlow, Z. Wang, H. Yan, A. K. Y. Jen, S. R. Marder, X. Zhan, *Nat. Rev. Mater.* **2018**, *3*, 18003.
[10] W. Jiang, Z. Liu, D. Zhu, W. Zheng, L. Chen, X. Zhang, G. Zhang, Y. Yi, L. Jiang, D. Zhang, *Angew. Chem. Int. Ed.***2021**, *60*, 10700–10708.
[11] Z. Ni, H. Dong, H. Wang, S. Ding, Y. Zou, Q. Zhao, Y. Zhen, F. Liu, L. Jiang, W. Hu, *Adv. Mater.* **2018**, *30*, 1704843.
[12] Y. Dong, Y. Sun, J. Liu, X. Shi, H. Li, J. Zhang, C. Li, Y. Yi, S. Mo, L. Fan, L. Jiang, *Adv. Sci.* **2022**, *9*, 2106085.
[13] H. Ebata, T. Izawa, E. Miyazaki, K. Takimiya, M. Ikeda, H. Kuwabara, T. Yui, *J. Am. Chem. Soc.* **2007**, *129*, 15732–15733.
[14] K. Sambe, T. Takeda, N. Hoshino, W. Matsuda, K. Shimada, K. Tsujita, S. Maruyama, S. Yamamoto, S. Seki, Y. Matsumoto, T. Akutagawa, *J. Am. Chem. Soc.* **2024**, *146*, 8557–8566.
[15] S. Kumagai, H. Ishii, G. Watanabe, C. P. Yu, S. Watanabe, J. Takeya, T. Okamoto, *Acc. Chem. Res.* **2022**, *55*, 660–672.
[16] D. Powell, X. Zhang, C. I. Nwachukwu, E. J. Miller, K. R. Hansen, L. Flannery, J. Ogle, A. Berzansky, J. G. Labram, A. G. Roberts, L. Whittaker-Brooks, *Adv. Mater.* **2022**, *34*, 2204656.
[17] L. Zhang, I. Song, J. Ahn, M. Han, M. Linares, M. Surin, H.-J. Zhang, J. H. Oh, J. Lin, *Nat. Commun.* **2021**, *12*, 142.
[18] Y. Zhang, S. H. Pun, Q. Miao, *Chem. Rev.* **2022**, *122*, 14554–14593.
[19] A. Borissov, Y. K. Maurya, L. Moshniaha, W.-S. Wong, M. Żyła-Karwowska, M. Tępień, *Chem. Rev.* **2022**, *122*, 565–788.
[20] P. F. Zhang, J. C. Zeng, F. D. Zhuang, K. X. Zhao, Z. H. Sun, Z. F. Yao, Y. Lu, X. Y. Wang, J. Y. Wang, J. Pei, *Angew. Chem. Int. Ed.* **2021**, *60*, 23313–23319.
[21] C. Duan, J. Zhang, J. Xiang, X. Yang, X. Gao, *Angew. Chem. Int. Ed.* **2022**, *61*, e202201494.
[22] A. Ong, T. Tao, Q. Jiang, Y. Han, Y. Ou, K. W. Huang, C. Chi, *Angew. Chem. Int. Ed.* **2022**, *61*, e202206286.
[23] S. Wang, M. Tang, L. Wu, L. Bian, L. Jiang, J. Liu, Z. B. Tang, Y. Liang, Z. Liu, *Angew. Chem. Int. Ed.* **2022**, *61*, e202205658.
[24] J. Wang, F. G. Gámez, J. Marín-Beloqui, A. Diaz-Andres, X. Miao, D. Casanova, J. Casado, J. Liu, *Angew. Chem. Int. Ed.* **2023**, *62*, e202217124.
[25] H. Xin, X. Gao, *ChemPlusChem* **2017**, *82*, 945–956.
[26] H. Xin, B. Hou, X. Gao, *Acc. Chem. Res.* **2021**, *54*, 1737–1753.
[27] F. Huang, M. Díaz-Fernández, J. M. Marín-Beloqui, L. Sun, Y. Chen, S. Liu, Y. Wang, H. Zheng, S. Li, C. Zhang, J. You, J. Casado, *J. Am. Chem. Soc.* **2025**, *147*, 1574–1583.
[28] L. Qin, Y. Y. Huang, B. Wu, J. Pan, J. Yang, J. Zhang, G. Han, S. Yang, L. Chen, Z. Yin, Y. Shu, L. Jiang, Y. Yi, Q. Peng, X. Zhou, C. Li, G. Zhang, X. S. Zhang, K. Wu, D. Zhang, *Angew. Chem. Int. Ed.* **2023**, *62*, e202304632.
[29] K. Yamamoto, Y. Ie, N. Tohnai, F. Kakiuchi, Y. Aso, *Sci. Rep.* **2018**, *8*, 17663.

[30] X. S. Zhang, Y. Y. Huang, J. Zhang, W. Meng, Q. Peng, R. Kong, Z. Xiao, J. Liu, M. Huang, Y. Yi, L. Chen, Q. Fan, G. Lin, Z. Liu, G. Zhang, L. Jiang, D. Zhang, *Angew. Chem. Int. Ed.* **2020**, *59*, 3529–3533.
[31] F. Zhou, W. Shi, X. Liao, Y. Yang, Z.-X. Yu, J. You, *ACS Catal.* **2022**, *12*, 676–686.
[32] R. Hatakenaka, N. Nishikawa, Y. Mikata, H. Aoyama, K. Yamashita, Y. Shiota, K. Yoshizawa, Y. Kawasaki, K. Tomooka, S. Kamijo, F. Tani, T. Murafuji, *Chem. Eur. J.* **2024**, *30*, e202400098.
[33] R. Hatakenaka, K. Urabe, S. Ueno, M. Yamauchi, Y. Mizuhata, H. Yamada, Y. Mikata, S. Kamijo, F. Tani, T. Murafuji, *Chem. Eur. J.* **2025**, *31*, e202404679.
[34] K. Yang, Z. Li, Y. Huang, Z. Zeng, *Acc. Chem. Res.* **2024**, *57*, 763–775.
[35] Y. Yang, Y. Wu, Z. Bin, C. Zhang, G. Tan, J. You, *J. Am. Chem. Soc.* **2024**, *146*, 1224–1243.
[36] C. Liu, J. Yuan, M. Gao, S. Tang, W. Li, R. Shi, A. Lei, *Chem. Rev.* **2015**, *115*, 12138–12204.
[37] I. A. Stepek, K. Itami, *ACS Mater. Lett.* **2020**, *2*, 951–974.
[38] A. L. Crombie, J. L. Kane, K. M. Shea, R. L. Danheiser, *J. Org. Chem.* **2004**, *69*, 8652–8667.
[39] D. Alberico, M. E. Scott, M. Lautens, *Chem. Rev.* **2007**, *107*, 174–238.
[40] C. M. Cardona, W. Li, A. E. Kaifer, D. Stockdale, G. C. Bazan, *Adv. Mater.* **2011**, *23*, 2367–2371.
[41] Deposition numbers These data are provided free of charge by the joint Cambridge Crystallographic Data Centre and Fachinformationszentrum Karlsruhe.
[42] C.-T. Hsieh, C.-Y. Chen, H.-Y. Lin, C.-J. Yang, T.-J. Chen, K.-Y. Wu, C.-L. Wang, *J. Phys. Chem. C* **2018**, *122*, 16242–16248.
[43] A. Pick, M. Klues, A. Rinn, K. Harms, S. Chatterjee, G. Witte, *Cryst. Growth Des.* **2015**, *15*, 5495–5504.
[44] M. Botoshansky, F. H. Herbstein, M. Kapon, *Helv. Chim. Acta* **2003**, *86*, 1113–1128.

Manuscript received: March 13, 2025
Revised manuscript received: May 12, 2025
Accepted manuscript online: May 12, 2025
Version of record online: May 22, 2025